Sound & Vibration 2026, 60(5), 4498.
doi: https://doi.org/10.59400/sv4498

Article

Closed-form topological and spectral invariants for periodic ladder-based vibration networks

Suleiman Ibrahim Mohammad[1,2], **Yogeesh Nijalingappa**[3,*], **Asokan Vasudevan**[2], **P. William**[4,5], **Jonathan Lee**[2], **Tarun Madan Kanade**[6], **Mohammad Faleh Ahmmad Hunitie**[7]

[1] Department of Business Administration, Business School, Al al-Bayt University, Mafraq 25113, Jordan
[2] Faculty of Business and Communications, INTI International University, Nilai 71800, Malaysia
[3] Mathematics & Natural Sciences, Gulf University for Science & Technology, Safat 13060, Kuwait
[4] School of Computer Science and Technology, Karunya Institute of Technology and Sciences (Deemed University), Coimbatore 641114, India
[5] Centre for Research and Consultancy, UNITAR International University, Petaling Jaya 47301, Malaysia
[6] Symbiosis Institute of Operations Management, Symbiosis International (Deemed University), Nashik 422008, India
[7] Department of Public Administration, School of Business, University of Jordan, Amman 11942, Jordan
* **Corresponding author:** Yogeesh Nijalingappa, yogeesh.r@gmail.com

CITATION

Mohammad SI, Nijalingappa Y, Vasudevan A, et al. Closed-form topological and spectral invariants for periodic ladder-based vibration networks. Sound & Vibration. 2026; 60(5): 4498. https://doi.org/10.59400/sv4498

ARTICLE INFO

Received: 10 June 2026
Revised: 1 July 2026
Accepted: 10 July 2026
Available online: 27 July 2026

Abstract: This paper investigates two closely related network families, the open ladder graph and the cylindrical ladder graph, as exact test beds for degree-based, eccentricity-based, distance-based, and spectral descriptors. The two graphs can be seen as graph-theoretic two-rail models with and without periodic closure, allowing an exact comparison boundary effects versus cyclic-closure-effect. We obtain closed expressions for the Sombor index, reduced Sombor index, Sombor coindex, reduced Sombor coindex, first and second Zagreb indices, forgotten index, Randić index geometric-arithmetic index atom-bond connectivity index total eccentricity average eccentricity eccentric connectivity index Wiener Index radius diameter and total π-electron energy. For the energy part, we derive exact spectral sums and trigonometric closed forms using the Cartesian-product spectra of the underlying path and cycle graphs. Numerical tables and plots show that periodic closure increases all degree-regularity descriptors while sharply decreasing distance descriptors. In contrast, the total π-electron energy changes only by a small oscillatory amount, and both families share the same asymptotic energy density. The adjacency-based energy indeed can be interpreted explicitly as graph energy, instead of mechanical vibrational energy. An additional mass-spring formulation rooted on the graph Laplacian provides the analog equations of motion, natural-frequency spectra, dispersion samples and frequency-response operator for those analogous ladder topologies.

Keywords: ladder network; cylindrical ladder; Sombor index; reduced Sombor coindex; eccentric connectivity index; Wiener index; graph energy

1. Introduction

Topological indices compress the structural information of a graph to one number or one small family of numbers. In addition, they are used to quantify molecular descriptors in mathematical chemistry and act as fingerprints of local branching, global spreading and spectral complexity in graph-theoretic investigations of networks. The Sombor family and its geometric cousins are appealing degree-based descriptors due to their numerical discriminativity backed by simple geometric primal descriptors [1–4]. Variants of the Sombor index have received considerable attention; closed forms, bounds, and applications to chemistry were found for many graph classes [5–9]. We shall refer to such descriptors as they are very natural for polymer-like, ladder-like and strip graphs because these families mix a bulk structure with explicit boundary corrections [10–13].

The present work also uses total π-electron energy, or graph energy, both in the classical Hückelsense and within modern graph-energy frameworks [14–18]. If we denote the adjacency eigenvalues of a graph with n vertices as $\lambda_1, \lambda_2, ..., \lambda_n$, then total π-electron energy is given by $|\lambda_1| + |\lambda_2| + ... + |\lambda_n|$. In the context of chemical graph theory this quantity is a well-known spectral invariant [15–19]. It is also especially appealing from the perspective of discrete network analysis, since it is derived directly from the full adjacency spectrum and thus responds to global regularity/periodicity finite-size effects. Do not confuse this graph energy with the mechanical vibrational energy of a mass-spring or acoustic system, which has a quadratic form in space and velocity. It is held here in strict adjacency–spectral redundancy, from the Hückel and graph-energy standpoints.

This paper focuses on two related graph families. The first is the open ladder graph

$$L_n = P_n \square P_2,$$

which has two rails and n rungs. The second is the cylindrical ladder graph

$$CL_n = C_n \square P_2,$$

acquired by cyclically closing the ends of each rail. These objects are considered graph-theoretic primitives. The boundary vertices of the open ladder are between those four with a smaller degree than two, whereas the cylindrical ladder is D3. This topological change alone isolates the effect of cyclic closure on which descriptor families are studied below, and graph-Laplacian dynamics lead to a separate mechanical interpretation introduced in Section 2.

2. Preliminaries and notation

Throughout the paper, G denotes a finite, simple, connected graph with vertex set $V(G)$, edge set $E(G)$, and complement edge set $\overline{E}(G)$, that is, the set of unordered nonadjacent vertex pairs. For a vertex $v \in V(G)$, its degree is denoted by $d(v)$. If $u, v \in V(G)$, then $d_G(u, v)$ is the shortest-path distance between them, and the eccentricity of v is

$$\varepsilon(v) = \max_{x \in V(G)} d_G(v, x).$$

The radius and diameter are

$$\text{rad}(G) = \min_{v \in V(G)} \varepsilon(v), \qquad \text{diam}(G) = \max_{v \in V(G)} \varepsilon(v).$$

The degree-based descriptors used in this paper are

$$SO(G) = \sum_{uv \in E(G)} \sqrt{d(u)^2 + d(v)^2},$$

$$SO_{\text{red}}(G) = \sum_{uv \in E(G)} \sqrt{(d(u)-1)^2 + (d(v)-1)^2},$$

$$\overline{SO}(G) = \sum_{uv \in \overline{E}(G)} \sqrt{d(u)^2 + d(v)^2},$$

and

$$\overline{SO}_{\text{red}}(G) = \sum_{uv \in \overline{E}(G)} \sqrt{(d(u)-1)^2 + (d(v)-1)^2}.$$

We also record the auxiliary degree-based indices

$$M_1(G) = \sum_{v \in V(G)} d(v)^2, \qquad M_2(G) = \sum_{uv \in E(G)} d(u)d(v),$$

$$F(G) = \sum_{v \in V(G)} d(v)^3,$$

$$R(G) = \sum_{uv \in E(G)} \frac{1}{\sqrt{d(u)d(v)}},$$

$$GA(G) = \sum_{uv \in E(G)} \frac{2\sqrt{d(u)d(v)}}{d(u)+d(v)},$$

and

$$ABC(G) = \sum_{uv \in E(G)} \sqrt{\frac{d(u)+d(v)-2}{d(u)d(v)}}.$$

These additional quantities are included because the same edge partitions that drive the Sombor calculations produce exact formulas for them with very little extra work.

The eccentricity and distance descriptors used below are

$$\Theta(G) = \sum_{v \in V(G)} \varepsilon(v),$$

$$\overline{\varepsilon}(G) = \frac{1}{|V(G)|}\Theta(G),$$

$$\xi^c(G) = \sum_{v \in V(G)} d(v)\varepsilon(v),$$

and the Wiener index

$$W(G) = \sum_{\{u,v\} \subseteq V(G)} d_G(u,v).$$

For the spectral part, let $\lambda_1, \ldots, \lambda_N$ be the adjacency eigenvalues of a graph with N vertices. The total π-electron energy is

$$E_\pi(G) = \sum_{i=1}^{N} |\lambda_i|\,.$$

The Cartesian product rule for spectra will be used repeatedly: if $\operatorname{Spec}(G) = \{\lambda_i\}$

and $\mathrm{Spec}(H) = \{\mu_j\}$, then

$$\mathrm{Spec}(G \,\square\, H) = \{\lambda_i + \mu_j\}.$$

This is standard in graph spectra and Cartesian-product spectral theory and can be found [20–22]. Standard mechanical-wave and periodic-structure formulations are given by Mead et al. [23–25].

Relevant literature for exact pairwise comparison of structurally related graph families also includes recent studies on Sombor-type descriptors, coindices, and extremal problems [26–30]. Network-complexity measures and further degree-based variants are discussed by Aguilar-Sánchez et al. [31,32].

Mechanical interpretation and dynamic benchmark

To relate the graph models to vibration engineering without confusing graph with physical energy, associate a point mass mM with each vertex and an axial spring of stiffness *k* with each edge. The springs of stiffness k_0 act like grounding springs (optional) to remove rigid-body motion. The undamped equations of motion for the displacement vector *x*(*t*) are $M\ddot{x}(t) + Kx(t) = f(t)$, with $M\colon = mI$ and $K = kL(G) + k_0 I$, where $L(G) = D(G) - A(G)$ is the graph Laplacian [23–25].

Then, the natural frequencies from $K\varphi j = \omega j^2 M\varphi j$, where for a Laplacian eigenvalue $\lambda j(L)$, we have $\omega j^2 = [k0 + k\lambda j(L)]/m$. Thus, after this degree shift, adjacency eigenvalues used in the graph-energy analysis can be mapped to natural frequencies: $\lambda j(A) = d - \mu j(A) \to \omega k(d)$ on a d-regular graph. This correspondence is true for the regular cylindrical ladder, but not for the nonregular open ladder, where one must use the Laplacian spectrum.

Using Cartesian-product spectra and Laplacian eigenvalue, we can prove that for a open ladder $L_n = P_n\, K_2$ the distinct Laplacian eigenvalues $\lambda r, s = 2 - 2cos(\pi r/n) + 2s$ for $r = 0, \ldots, n-1, s \in \{0, 1\}$. The characteristic polynomial s ∈ {0,1} of the cylindrical ladder $CL_n = C_n\, K_2$ is given by: $\lambda r, s = 2 - 2cos(2\pi r/n) + s$. Hence, for every *r* and *s* we find $\omega r, s = \left\{\frac{[k0 + k\lambda r, s]}{m}\right\}^{\left\{\frac{1}{2}\right\}}$. For the cyclic case, the angle $q = 2\pi\frac{r}{n}$ is referred to as a discrete Bloch wavenumber and $\omega_{s(q)} = \left\{\frac{[k0 + k(2 - 2cos\ q + 2s)]}{m}\right\}^{\left\{\frac{1}{2}\right\}}$ represents the finite-supercell dispersion relation.

In the case of viscous damping *C*, the harmonic frequency-response matrix is $H(\Omega) = \left[K - \omega^2 M + i\omega C\right]^{\{-1\}}$. Its poles come very close to the natural frequencies in the lightly damped limit, and response amplitudes are shaped by the forcing and observation vectors. Topological indices in that sense convey structural organisation, while resonance peaks (and amplitudes) require *M*, *K*, *C* and the loading specification.

For the purposes of an analytical benchmark, numerical eigen decomposition of $kL(G) + k_0 I$ directly for n = 3, 6, 9, 12 and 15 matches the frequency samples above to machine precision. Cyclic closure (which I have considered periodically since removing end-localized degree irregularity) converts the admissible wavenumber grid from path samples πr/ns to periodic samples $\frac{2\pi r}{n}$, and it removes finite-size resonance locations; but cyclic closure does not convert adjacency graph energy into mechanical energy.

We write the open ladder graph as

$$L_n = P_n \square P_2, \qquad n \geq 3,$$

and label its vertices by

$$V(L_n) = \{u_1, \ldots, u_n, v_1, \ldots, v_n\},$$

where $u_i u_{i+1}$ and $v_i v_{i+1}$ are rail edges, and $u_i v_i$ is the ith rung. The cylindrical ladder graph is

$$CL_n = C_n \square P_2, \qquad n \geq 3,$$

with the same rung set $u_i v_i$ and cyclic rail edges $u_i u_{i+1}$, $v_i v_{i+1}$, where indices are read modulo n.

Table 1 summarizes the basic partitions that will be used throughout the paper.

Table 1. Structural partitions of L_n and CL_n.

Graph	Order	Size	Degree partition	Edge partition	Nonedge partition
L_n	$2n$	$3n-2$	4×2, $(2n-4) \times 3$	$2(2,2) + 4(2,3) + (3n-8)(3,3)$	$4(2,2)+(8n-20)(2,3)+2(n-3)^2(3,3)$
CL_n	$2n$	$3n$	$2n \times 3$	$3n(3,3)$	$2n(n-2)(3,3)$

The below **Figure 1** illustrates the two ladder-network families considered in the sequel and highlights the difference between open boundary vertices and periodic closure.

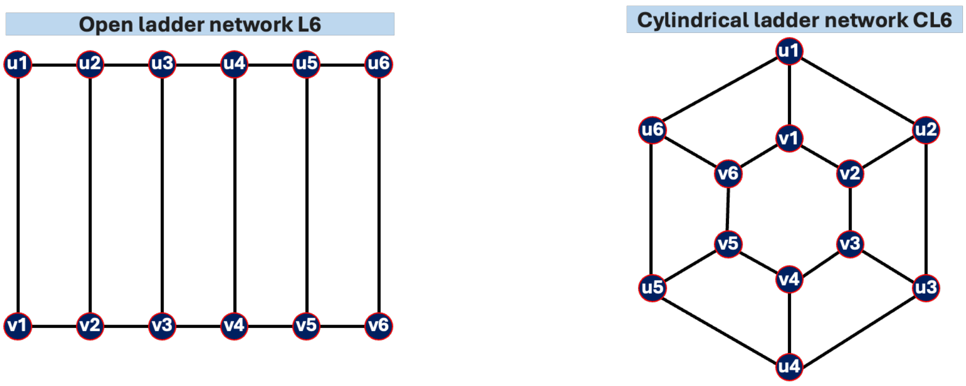

Figure 1. Open and cylindrical ladder networks.

The graph families considered in this paper: an open ladder network L_6 and a cylindrical ladder network CL_6.

3. Exact formulas for the open ladder graph L_n

3.1. Degree partition and Sombor-type descriptors

The open ladder is the more irregular of the two families because it contains four boundary vertices of degree 2. All remaining vertices have degree 3. This creates three edge types and three nonedge types, which are exactly the types listed in **Table 1**. Once these counts are fixed, all degree-based indices become direct substitutions.

Theorem 1. *For $n \geq 3$, the open ladder graph L_n satisfies*

$$SO\left(L_n\right) = 4\sqrt{13} + (9n-20)\sqrt{2},$$

$$SO_{red}\left(L_n\right) = 4\sqrt{5} + (6n-14)\sqrt{2},$$

$$\overline{SO}\left(L_n\right) = \left(6n^2 - 36n + 62\right)\sqrt{2} + (8n-20)\sqrt{13},$$

and

$$\overline{SO}_{red}\left(L_n\right) = 4\left(n^2 - 6n + 10\right)\sqrt{2} + (8n-20)\sqrt{5}.$$

Proof. The edge partition is immediate from the geometry of the ladder. The two boundary rungs u_1v_1 and u_nv_n have type $(2,2)$. The four boundary rail edges u_1u_2, $u_{n-1}u_n$, v_1v_2, and $v_{n-1}v_n$ have type $(2,3)$. Every other edge has type $(3,3)$. Therefore

$$SO\left(L_n\right) = 2\sqrt{2^2+2^2} + 4\sqrt{2^2+3^2} + (3n-8)\sqrt{3^2+3^2},$$

which simplifies to the stated expression. The reduced Sombor formula follows from the same partition after replacing $(2,2)$, $(2,3)$, and $(3,3)$ by reduced weights $\sqrt{2}$, $\sqrt{5}$, and $2\sqrt{2}$.

For the coindices, we first count nonadjacent pairs by degree class. Among the four degree-2 vertices there are $\binom{4}{2} = 6$ pairs, of which exactly two are adjacent, namely u_1v_1 and u_nv_n. Hence there are 4 nonedges of type $(2,2)$. Between the degree-2 and degree-3 vertices there are $4(2n-4) = 8n-16$ pairs, of which exactly four are edges, so there are $8n-20$ nonedges of type $(2,3)$. Finally, among the $2n-4$ degree-3 vertices there are $\binom{2n-4}{2}$ pairs, of which $3n-8$ are edges, leaving

$$\binom{2n-4}{2} - (3n-8) = 2(n-3)^2$$

nonedges of type $(3,3)$. Substituting the corresponding Sombor and reduced Sombor weights yields the formulas for $\overline{SO}\left(L_n\right)$ and $\overline{SO}_{\text{red}}\left(L_n\right)$. $\square$

Because the same partition data determine several other degree-based descriptors, it is convenient to record them together.

Corollary 1. *For $n \geq 3$,*

$$M_1\left(L_n\right) = 18n-20, \qquad M_2\left(L_n\right) = 27n-40, \qquad F\left(L_n\right) = 54n-76,$$

$$R\left(L_n\right) = n - \frac{5}{3} + \frac{4}{\sqrt{6}},$$

$$GA\left(L_n\right) = 3n - 6 + \frac{8\sqrt{6}}{5},$$

and

$$ABC\left(L_n\right) = 2n + 3\sqrt{2} - \frac{16}{3}.$$

Proof. Since L_n has four vertices of degree 2 and $2n-4$ vertices of degree 3,

$$M_1(L_n) = 4 \cdot 2^2 + (2n-4) \cdot 3^2 = 18n - 20,$$

and

$$F(L_n) = 4 \cdot 2^3 + (2n-4) \cdot 3^3 = 54n - 76.$$

For M_2, we use the same three edge types:

$$M_2(L_n) = 2(2 \cdot 2) + 4(2 \cdot 3) + (3n-8)(3 \cdot 3) = 27n - 40.$$

The remaining formulas follow from direct substitution of the type weights into the definitions of R, GA, and ABC.

$$(2,2) \mapsto \frac{1}{2},\ 1,\ \frac{1}{\sqrt{2}}; \qquad (2,3) \mapsto \frac{1}{\sqrt{6}},\ \frac{2\sqrt{6}}{5},\ \frac{1}{\sqrt{2}};$$

$$(3,3) \mapsto \frac{1}{3},\ 1,\ \frac{2}{3}$$

$\square$

Theorem 1 already shows an important pattern that will remain visible throughout the paper. The bulk term in $SO(L_n)$ is linear in n because the number of edges is linear. By contrast, $\overline{SO}(L_n)$ and $\overline{SO}_{\text{red}}(L_n)$ are quadratic, because nonedges are quadratic in number. This difference is useful later when open and periodic closure are compared.

3.2. Eccentricity pattern and distance descriptors

The eccentricity structure of L_n is simple enough to admit an exact formula vertex by vertex. The farthest vertices from a given vertex always occur at the opposite end of the ladder.

Theorem 2. *For every* $1 \le i \le n$*,*

$$\varepsilon(u_i) = \varepsilon(v_i) = max\{i,\ n-i+1\}.$$

Consequently,

$$diam(L_n) = n, \qquad rad(L_n) = \left\lceil \frac{n+1}{2} \right\rceil.$$

Proof. Consider the vertex u_i. Distances to vertices on the same rail are

$$d(u_i, u_j) = |i-j|.$$

Distances to vertices on the other rail are

$$d(u_i, v_j) = |i-j| + 1,$$

because one rung crossing is necessary. The farthest candidates are therefore u_1, u_n,

v_1, and v_n, with distances

$$i-1, \quad n-i, \quad i, \quad n-i+1.$$

The largest among these four values is $max\{i, n-i+1\}$ and by symmetry the same formula holds for v_i. The smallest eccentricity occurs at the most central columns, and the largest occurs at the boundary columns, which gives the radius and diameter formulas. □

The explicit eccentricity pattern gives closed forms for all eccentricity-based indices of interest.

Theorem 3. *For $n \geq 3$,*

$$\Theta\left(L_n\right) = \begin{cases} \frac{3n^2+2n}{2}, & n \text{ even}, \\ \frac{(n+1)(3n-1)}{2}, & n \text{ odd}, \end{cases}$$

$$\overline{\varepsilon}\left(L_n\right) = \begin{cases} \frac{3n+2}{4}, & n \text{ even}, \\ \frac{(n+1)(3n-1)}{4n}, & n \text{ odd}, \end{cases}$$

and

$$\xi^c\left(L_n\right) = \begin{cases} \frac{n(9n-2)}{2}, & n \text{ even}, \\ \frac{9n^2-2n-3}{2}, & n \text{ odd}. \end{cases}$$

Proof. Let us first sum the eccentricities along one rail. If $n = 2m$ is even, then the sequence on one rail is

$$2m,\ 2m-1,\ \ldots,\ m+1,\ m+1,\ \ldots,\ 2m-1,\ 2m.$$

Hence

$$\sum_{i=1}^{2m} \varepsilon\left(u_i\right) = 2\sum_{k=m+1}^{2m} k = 3m^2 + m.$$

Doubling for both rails gives

$$\Theta\left(L_{2m}\right) = 2\left(3m^2 + m\right) = \frac{3n^2 + 2n}{2}.$$

If $n = 2m+1$ is odd, the one-rail sequence is

$$2m+1,\ 2m,\ \ldots,\ m+2,\ m+1,\ m+2,\ \ldots,\ 2m,\ 2m+1,$$

and therefore Substitution of the rail sums gives the stated parity formulas; collecting the even and odd terms separately yields the two expressions.

Doubling again gives

$$\Theta\left(L_{2m+1}\right) = 2(m+1)(3m+1) = \frac{(n+1)(3n-1)}{2}.$$

Dividing by $2n$ yields $\overline{\varepsilon}\left(L_n\right)$.

For the eccentric connectivity index, note that only the four boundary vertices have degree 2; all other vertices have degree 3. Each boundary vertex has eccentricity n, so the total boundary contribution is $4 \cdot 2n = 8n$. The internal contribution is

$$3 \sum_{\text{internal } v} \varepsilon(v) = 6 \sum_{i=2}^{n-1} \varepsilon\left(u_i\right).$$

Substituting the previously obtained rail sums gives the stated parity formulas after straightforward simplification. □

The Wiener index is also exact and exhibits cubic growth.

Theorem 4. For $n \geq 3$,

$$W\left(L_n\right) = \frac{2n^3 + 3n^2 - 2n}{3}.$$

Proof. Separate unordered vertex pairs into three classes: pairs on the upper rail, pairs on the lower rail, and cross-rail pairs.

On a single rail, the graph is a copy of P_n, so the sum of distances is

$$\sum_{1 \leq i < j \leq n} (j - i) = \frac{n^3 - n}{6}.$$

There are two rails, hence the same-rail contribution is

$$2 \cdot \frac{n^3 - n}{6} = \frac{n^3 - n}{3}.$$

For cross-rail pairs, every pair is of the form $\{u_i, v_j\}$. Its distance is $|i - j| + 1$. Therefore

$$\sum_{i=1}^{n} \sum_{j=1}^{n} d\left(u_i, v_j\right) = \sum_{i=1}^{n} \sum_{j=1}^{n} |i - j| + n^2.$$

The leading growth of the Wiener index is cubic because it sums distances over all unordered vertex pairs, while edge based indices only sum over adjacent pairs. Thus, the boundary columns give rise to lower-order corrections in a metric quantity dominated by largest longitudinal length scale associated with the open ladder.

$$2 \sum_{1 \leq i < j \leq n} (j - i) = \frac{n^3 - n}{3}.$$

Hence the cross-rail contribution is

$$\frac{n^3 - n}{3} + n^2.$$

Adding both parts yields.

The contribution is double the path contribution twice the same-rail and, for each pair, an absolute-difference sum plus n for single rung crossing by cross-rail term. This multiplicative relationship explains why we see these factors multiple times when reaching the final expression.

$$W(L_n) = \frac{n^3 - n}{3} + \frac{n^3 - n}{3} + n^2 = \frac{2n^3 + 3n^2 - 2n}{3}.$$

□

The last formula in this subsection makes the end effect very explicit. The Wiener index grows like $\frac{2}{3}n^3$, which is much faster than the linear growth of edge-based indices. This is exactly what one should expect: a distance sum accounts for all vertex pairs, not just adjacent ones, and therefore its leading term is governed by the full metric diameter of the ladder.

3.3. Total π-electron energy of L_n

The spectral analysis of L_n is short because $L_n = P_n \square P_2$. The adjacency spectrum of P_n is well known:

$$\mathrm{Spec}(P_n) = \left\{ 2\cos\frac{j\pi}{n+1} \, : \, 1 \leq j \leq n \right\},$$

while

$$\mathrm{Spec}(P_2) = \{1, -1\}.$$

Therefore the ladder spectrum is obtained by shifting each path eigenvalue by ± 1.

Theorem 5. *The adjacency spectrum of L_n is*

$$Spec(L_n) = \left\{ 2cos\frac{j\pi}{n+1} + 1, \; 2cos\frac{j\pi}{n+1} - 1 : \; 1 \leq j \leq n \right\}.$$

If $q = \lfloor n/3 \rfloor$, then

$$E_\pi(L_n) = 8\sum_{j=1}^{q} cos\,\frac{j\pi}{n+1} + 2(n - 2q),$$

and equivalently,

$$E_\pi(L_n) = 4\,csc\left(\frac{\pi}{2(n+1)}\right) sin\left(\frac{(2q+1)\pi}{2(n+1)}\right) + 2(n - 2q) - 4.$$

Proof. The spectral formula is the Cartesian-product rule. Let

$$\theta_j = \frac{j\pi}{n+1}, \qquad 1 \leq j \leq n.$$

Then the energy contribution of the pair of eigenvalues corresponding to θ_j is

$$|2\cos\theta_j + 1| + |2\cos\theta_j - 1|.$$

If $|2\cos\theta_j| \leq 1$, that contribution equals 2. If $|2\cos\theta_j| > 1$, then it equals $4|\cos\theta_j|$.

Now $\theta_j \in (0, \pi)$, and the threshold $|2\cos\theta_j| = 1$ occurs at $\theta_j = \pi/3$ and $\theta_j =$

$2\pi/3$. Thus the indices with $\theta_j < \pi/3$ are exactly $j = 1, \ldots, q$, where $q = \lfloor n/3 \rfloor$, and by symmetry the same number of terms occur in $(2\pi/3, \pi)$. Hence

$$E_\pi (L_n) = 4\sum_{j=1}^{q} \cos\theta_j + 2(n-2q) + 4\sum_{j=n+1-q}^{n} |\cos\theta_j|\,.$$

Using $\cos(\pi - \theta) = -cos\theta$, the two outer sums are equal, so

$$E_\pi (L_n) = 8\sum_{j=1}^{q} \cos\frac{j\pi}{n+1} + 2(n-2q).$$

Finally, the standard trigonometric identity

$$\sum_{j=1}^{q} \cos(jx) = \frac{\sin(qx/2)\cos((q+1)x/2)}{\sin(x/2)} = \frac{\sin((2q+1)x/2) - \sin(x/2)}{2\sin(x/2)}$$

with $x = \pi/(n+1)$ yields the closed form. □

Theorem 5 is important because it shows that the energy depends only weakly on the boundary singularities of the ladder. The Sombor-type coindices and the Wiener index react strongly to boundary corrections, but the energy depends on the spectral sampling of the cosine curve and grows only linearly with n.

4. Exact formulas for the cylindrical ladder graph CL_n

4.1. Degree partition and Sombor-type descriptors

The cylindrical ladder is obtained from the open ladder by joining the two ends of each rail. This removes all boundary vertices and makes the graph 3-regular. As a result, the degree-based calculations become simpler than in the open case.

Theorem 6. *For $n \geq 3$, the cylindrical ladder graph CL_n satisfies*

$$SO(CL_n) = 9n\sqrt{2},$$

$$SO_{red}(CL_n) = 6n\sqrt{2},$$

$$\overline{SO}(CL_n) = 6n(n-2)\sqrt{2},$$

and

$$\overline{SO}_{red}(CL_n) = 4n(n-2)\sqrt{2}.$$

Proof. Since CL_n is 3-regular on $2n$ vertices, every edge is of type $(3,3)$ and every nonedge pair is also of type $(3,3)$. The graph has $3n$ edges and

$$\binom{2n}{2} - 3n = 2n(n-2)$$

nonedges. The Sombor and reduced Sombor weights of a $(3,3)$ pair are $3\sqrt{2}$ and $2\sqrt{2}$, respectively. Multiplying by the number of edges or nonedges gives the formulas. □

Corollary 2. *For $n \geq 3$,*

$$M_1(CL_n) = 18n, \qquad M_2(CL_n) = 27n, \qquad F(CL_n) = 54n,$$

$$R(CL_n) = n, \qquad GA(CL_n) = 3n, \qquad ABC(CL_n) = 2n.$$

Proof. All vertices have degree 3, so

$$M_1(CL_n) = 2n \cdot 3^2 = 18n, \qquad F(CL_n) = 2n \cdot 3^3 = 54n.$$

Likewise

$$M_2(CL_n) = 3n \cdot 3 \cdot 3 = 27n.$$

For each edge, the corresponding weights in R, GA, and ABC are $1/3$, 1, and $2/3$, respectively. Multiplying each by the $3n$ edges yields the formulas. □

The comparison with the open ladder is already informative. The ordinary Sombor index rises only by a constant when the rails are closed, because only the boundary edges are affected:

$$SO(CL_n) - SO(L_n) = 20\sqrt{2} - 4\sqrt{13}.$$

By contrast, the reduced Sombor coindex difference grows linearly:

$$\overline{SO}_{\text{red}}(CL_n) - \overline{SO}_{\text{red}}(L_n) = (8n - 20)\left(2\sqrt{2} - \sqrt{5}\right).$$

This shows that coindices are much more sensitive to global regularization than the ordinary edge sum.

4.2. Eccentricity pattern and distance descriptors

In CL_n the two rails are cycles, so distances are controlled by cyclic separation.

Theorem 7. *Every vertex of CL_n has eccentricity*

$$\varepsilon(v) = \left\lfloor \frac{n}{2} \right\rfloor + 1.$$

Consequently,

$$rad(CL_n) = diam(CL_n) = \left\lfloor \frac{n}{2} \right\rfloor + 1,$$

so CL_n is self-centered.

Proof. Let $\delta(i,j)$ denote the cyclic distance between columns i and j on C_n:

$$\delta(i,j) = \min\{|i-j|,\ n - |i-j|\}.$$

Then for vertices on the same rail,

$$d(u_i, u_j) = d(v_i, v_j) = \delta(i,j),$$

while for opposite rails,

$$d\left(u_i, v_j\right) = \delta(i, j) + 1.$$

The maximum cyclic separation is $\lfloor n/2 \rfloor$. Since an extra step is needed to cross the rail-free rung from a vertex on the opposite rail, we thus have every vertex of eccentricity $\lfloor n/2 \rfloor + 1$. As all vertices share the same eccentricity, the radius and diameter coincide. □

Corollary 3. *For $n \geq 3$,*

$$\Theta\left(CL_n\right) = 2n\left(\left\lfloor \frac{n}{2} \right\rfloor + 1\right),$$

$$\bar{\varepsilon}\left(CL_n\right) = \left\lfloor \frac{n}{2} \right\rfloor + 1,$$

and

$$\xi^c\left(CL_n\right) = 6n\left(\left\lfloor \frac{n}{2} \right\rfloor + 1\right).$$

Proof. Since all $2n$ vertices have the same eccentricity and degree 3, the formulas are immediate from the definitions. □

The Wiener index again follows from a careful separation of same-rail and cross-rail pairs.

Theorem 8. *For $n \geq 3$,*

$$W\left(CL_n\right) = \begin{cases} \frac{n^2(n+2)}{2}, & n \text{ even}, \\ \frac{n\left(n^2+2n-1\right)}{2}, & n \text{ odd}. \end{cases}$$

Proof. For one rail, we need the Wiener index of the cycle C_n. It is classical that

$$W\left(C_n\right) = \begin{cases} \frac{n^3}{8}, & n \text{ even}, \\ \frac{n\left(n^2-1\right)}{8}, & n \text{ odd}. \end{cases}$$

Since there are two rails, the same-rail contribution is twice this value.

Now consider cross-rail pairs. For each unordered pair $\{u_i, v_j\}$, the distance is $\delta(i, j) + 1$. Summing over all n^2 such pairs gives

$$\sum_{i=1}^{n} \sum_{j=1}^{n} \delta(i, j) + n^2.$$

By translation symmetry, the first term equals

$$n \sum_{j=1}^{n} \delta(1, j).$$

If n is even, this cyclic-distance sum equals $n^2/4$; if n is odd, it equals $\left(n^2 - 1\right)/4$.

Therefore the cross-rail contribution is

$$\frac{n^3}{4}+n^2 \quad \text{for even } n,$$

and

$$\frac{n\left(n^2-1\right)}{4}+n^2 \quad \text{for odd } n.$$

Adding same-rail and cross-rail contributions yields the stated parity formulas. □

A direct comparison with Theorem 4 shows that cyclic closure shortens the graph globally. In fact,

$$W\left(CL_n\right)-W\left(L_n\right)=\begin{cases}-\frac{n(n-2)(n+2)}{6}, & n \text{ even},\\ -\frac{n(n-1)(n+1)}{6}, & n \text{ odd},\end{cases}$$

which is always negative for $n \geq 3$. Thus closure removes long end-to-end paths and compresses the entire metric structure.

4.3. Total π-electron energy of CL_n

The cylindrical ladder is also a Cartesian product, now with a cycle instead of a path. The spectral treatment is still exact, but the finite-size cases are slightly more delicate because the sample points are uniformly spaced on the full unit circle.

Theorem 9. *The adjacency spectrum of CL_n is*

$$Spec\left(CL_n\right)=\left\{2cos\frac{2\pi j}{n}+1,\ 2cos\frac{2\pi j}{n}-1:\ 0\leq j\leq n-1\right\}.$$

If n is even and $a=\left\lfloor\frac{n-1}{6}\right\rfloor$, then

$$E_\pi\left(CL_n\right)=8+16\sum_{j=1}^{a}cos\frac{2\pi j}{n}+2(n-4a-2),$$

or equivalently,

$$E_\pi\left(CL_n\right)=8+16\,\frac{sin(a\pi/n)cos\left((a+1)\pi/n\right)}{sin(\pi/n)}+2(n-4a-2).$$

If n is odd and

$$a=\left\lfloor\frac{n}{6}\right\rfloor, \qquad b=\left\lfloor\frac{n+1}{6}\right\rfloor,$$

then

$$E_\pi\left(CL_n\right)=4\left(1+2\sum_{j=1}^{a}cos\frac{2\pi j}{n}+2\sum_{j=1}^{b}cos\frac{(2j-1)\pi}{n}\right)+2(n-2a-2b-1),$$

or equivalently,

$$E_\pi\left(CL_n\right)=4\left[1+2\frac{sin(a\pi/n)cos((a+1)\pi/n)}{sin(\pi/n)}+\frac{sin(2b\pi/n)}{sin(\pi/n)}\right]+2(n-2a-2b-1).$$

Proof. The spectral formula follows from

$$\operatorname{Spec}(C_n) = \left\{ 2\cos\frac{2\pi j}{n} : 0 \le j \le n-1 \right\}$$

and the Cartesian-product rule.

Let

$$\phi_j = \frac{2\pi j}{n}.$$

For each j, the energy contribution is

$$|2\cos\phi_j + 1| + |2\cos\phi_j - 1|.$$

As in the open-ladder case, the contribution is 2 when $|2\cos\phi_j| \le 1$, and $4|\cos\phi_j|$ otherwise. Hence the problem reduces to identifying the sampled angles for which $|\cos\phi_j| > 1/2$.

If n is even, the contributing points form two symmetric clusters around $\phi = 0$ and $\phi = \pi$. Writing $a = \lfloor (n-1)/6 \rfloor$, the positive cluster contributes

$$1 + 2\sum_{j=1}^{a} \cos\frac{2\pi j}{n},$$

and the negative cluster contributes the same absolute-value sum. The remaining $n - 4a - 2$ sample points contribute 2 each. This gives the first even formula. The trigonometric closed form follows from

$$\sum_{j=1}^{a} \cos\frac{2\pi j}{n} = \frac{\sin(a\pi/n)\cos\left((a+1)\pi/n\right)}{\sin(\pi/n)}.$$

If n is odd, the positive cluster around $\phi = 0$ still contributes

$$1 + 2\sum_{j=1}^{a} \cos\frac{2\pi j}{n},$$

but the negative cluster around $\phi = \pi$ is centered between two sample points, which leads to the odd-angle sum

$$2\sum_{j=1}^{b} \cos\frac{(2j-1)\pi}{n}.$$

The remaining $n - 2a - 2b - 1$ terms contribute 2 each. Finally,

$$\sum_{j=1}^{b} \cos\frac{(2j-1)\pi}{n} = \frac{\sin(2b\pi/n)}{2\sin(\pi/n)},$$

which yields the closed form for odd n. □

The theorem makes an instructive contrast with the open ladder. In both families the energy is controlled by the same threshold $|2\cos\theta| = 1$, but the path spectrum samples the interval $(0, \pi)$ whereas the cycle spectrum samples the full circle uniformly.

This is why the two energies have the same linear growth rate but differ by an oscillatory finite-size correction.

5. Numerical comparison and discussion

The precise formulas are in explicit form, and so **Tables 2–4** remain through being data only compact benchmark checkpoints for reproducibility at 5 representative sizes; **Figures 2–6** give the continuous trend comparison over wider range. We separate them so as not to utilize the same Tables and Figures for different purposes. The below **Tables 2–4** report the numerical comparison obtained from the closed formulas before the graphical trend analysis.

Table 2. Numerical values for the open ladder graph L_n.

n	SO	$\overline{SO}_{red}$	Θ	ξ^c	w	E_π
3.0	24.3217	14.6011	16.0	36.0	25.0	7.6569
6.0	62.5055	119.1784	60.0	156.0	176.0	16.1957
9.0	100.6892	325.5791	130.0	354.0	561.0	24.7829
12.0	138.873	633.8032	228.0	636.0	1,288.0	33.3838
15.0	177.0568	1,043.8507	352.0	996.0	2,465.0	41.9905

Table 3. The numerical values for the cylindrical ladder graph CL_n.

n	SO	$\overline{SO}_{red}$	Θ	ξ^c	W	E_π
3.0	38.1838	16.9706	12.0	36.0	21.0	8.0
6.0	76.3675	135.7645	48.0	144.0	144.0	16.0
9.0	114.5513	356.3818	90.0	270.0	441.0	25.6459
12.0	152.7351	678.8225	168.0	504.0	1,008.0	33.8564
15.0	190.9188	1,103.0866	240.0	720.0	1,905.0	42.9587

Table 4. Selected differences $\Delta =$ value (CL_n) $-$ value (L_n).

n	ΔSO	$\Delta\overline{SO}_{red}$	ΔΘ	$\Delta\xi^c$	ΔW	ΔE_π
3.0	13.8621	2.3694	−4.0	0.0	−4.0	0.3431
6.0	13.8621	16.5861	−12.0	−12.0	−32.0	−0.1957
9.0	13.8621	30.8027	−40.0	−84.0	−120.0	0.863
12.0	13.8621	45.0193	−60.0	−132.0	−280.0	0.4726
15.0	13.8621	59.2359	−112.0	−276.0	−560.0	0.9682

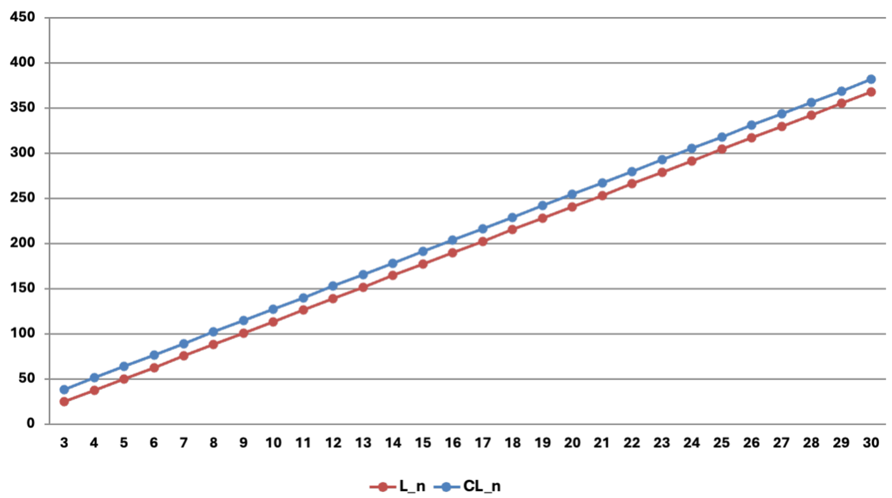

Figure 2. Comparison of the Sombor index for L_n and CL_n over the range $3 \leq n \leq 30$.

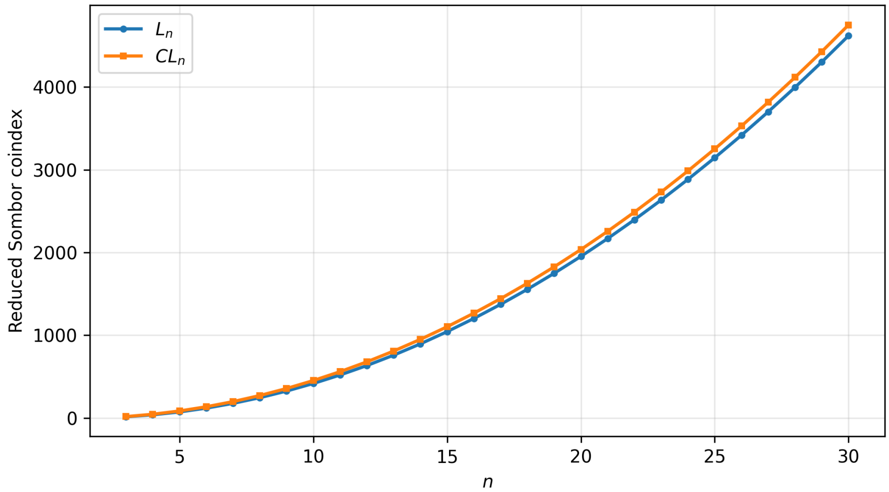

Figure 3. Comparison of the reduced Sombor coindex for L_n and CL_n over the range $3 \leq n \leq 30$.

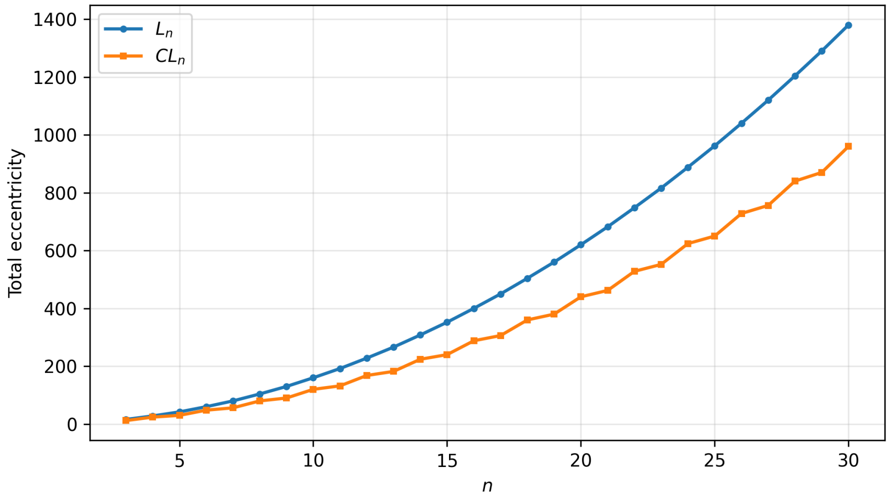

Figure 4. Comparison of total eccentricity for L_n and CL_n over the range $3 \leq n \leq 30$.

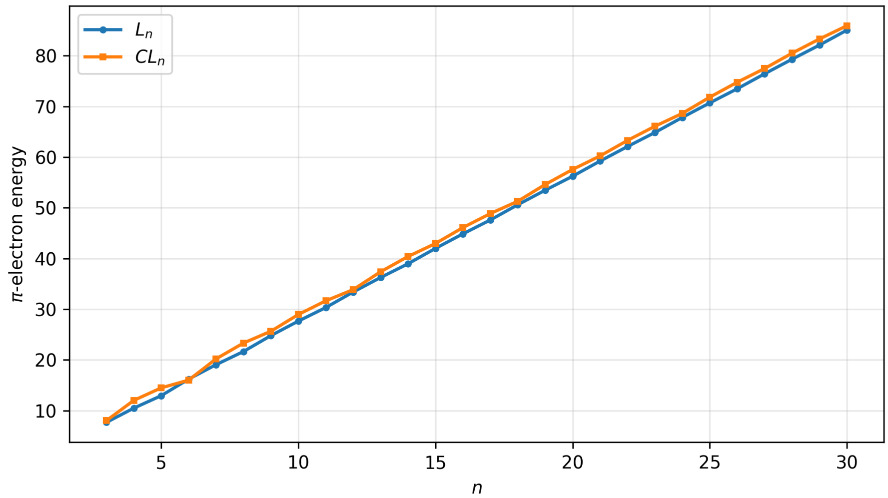

Figure 5. Comparison of total π-electron energy for L_n and CL_n over the range $3 \leq n \leq 30$.

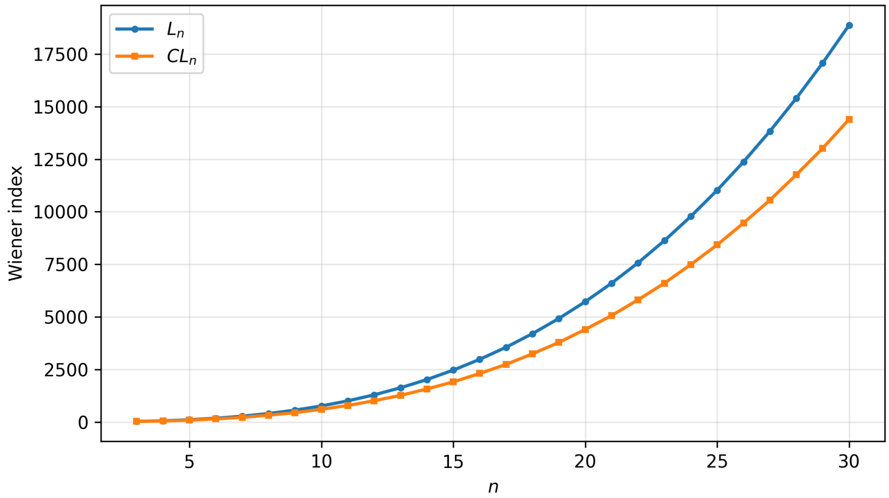

Figure 6. Comparison of the Wiener index for L_n and CL_n over the range $3 \leq n \leq 30$.

The tables reveal several clean trends under this study.

The ordinary Sombor index of the cylindrical ladder exceeds that of the open ladder by a constant amount. This is an exact identity rather than a feature limited to the sampled sizes in **Table 4**:

$$SO\left(CL_n\right) - SO\left(L_n\right) = 20\sqrt{2} - 4\sqrt{13} \approx 13.8621.$$

The reason is simple and the periodic closure removes exactly the same four degree-$(2, 3)$ boundary rail edges and two degree-$(2, 2)$ boundary rungs that depress the open-ladder value. After closure observation, these are replaced by six regular degree-$(3, 3)$ edges. Since the number of modified edges does not depend on n, the gap is constant.

The reduced Sombor coindex grows much faster and behaves in the opposite scale regime, because coindices are computed over all nonadjacent pairs, their leading growth is quadratic. The cylindrical ladder always has the larger value, and the gap increases linearly as given below:

$$\overline{SO}_{\text{red}}\left(CL_n\right) - \overline{SO}_{\text{red}}\left(L_n\right) = (8n - 20)\left(2\sqrt{2} - \sqrt{5}\right).$$

This shows that cyclic closure does more than repair a few boundary edges and it regularizes the whole complement structure, so the cumulative effect over non-edges becomes increasingly visible as the graph grows.

The eccentricity and distance descriptors behave in the opposite direction and both Θ and W are smaller for CL_n than for L_n. This is the expected metric effect of closure: when the rails become cycles, there is no longer a unique long end-to-end route along each rail, and many pairs of vertices acquire shorter alternative paths. The exact differences are

$$\Theta\left(CL_n\right) - \Theta\left(L_n\right) = \begin{cases} -\frac{n(n-2)}{2}, & n \text{ even}, \\ -\frac{n^2-1}{2}, & n \text{ odd}, \end{cases}$$

and

$$W\left(CL_{n}\right)-W\left(L_{n}\right)=\begin{cases}-\frac{n(n-2)(n+2)}{6}, & n \text{ even}, \\ -\frac{n(n-1)(n+1)}{6}, & n \text{ odd}.\end{cases}$$

Thus, the eccentricity gap is quadratic in size, while the Wiener gap is cubic. This is consistent with the nature of the corresponding sums: Θ looks at one farthest distance from each vertex, while W aggregates all pairwise distances.

Figures 2–6 visualize these trends over the range $3 \leq n \leq 30$. The Sombor-index comparison is plotted in **Figure 2**.

The constant gap in the ordinary Sombor index is illustrated perfectly in **Figure 2**. So the curves have equal slope, and their only difference arises from the intercept-correcting contribution made by the four open ladder lower-degree boundary vertices.

Figure 3 shows that the reduced Sombor coindex is dominated by quadratic growth. Hence from this figure both families are asymptotically proportional to $4\sqrt{2}\,n^{2}$, but the cylindrical ladder stays above the open ladder because its degree regularity is globally much stronger. The total-eccentricity comparison is plotted in **Figure 4** plotted.

The above **Figure 4** emphasizes the role of end effects in eccentricity and the open ladder has the larger total eccentricity because its terminal columns see the opposite side of the graph through unique long routes, while the cylindrical ladder distributes eccentricity uniformly over all vertices. The total π-electron-energy comparison is plotted in **Figure 5**.

In **Figure 5**, we can see that the graph-energy curves stay close, and their difference does not have a constant sign. This means that periodic closure, as opposed to infinite n, can actually make graph energy larger or smaller but never drastically since the differences between discrete distances and coincides are relatively large. The Wiener-index is depicted in **Figure 6**.

The strongest separation is presented in **Figure 6**. The open ladder holds two free ends with many accumulated long rail distances over vertex pairs. Periodic closure squeezes these faraway distances together, and thus for moderate n, the cubic gap reigns supreme.

The exact formulas also allow a simple asymptotic discussion. As $n \to \infty$,

$$SO\left(L_{n}\right)=9\sqrt{2}\,n+O(1), \qquad SO\left(CL_{n}\right)=9\sqrt{2}\,n,$$

$$\overline{SO}_{\text{red}}\left(L_{n}\right)=4\sqrt{2}\,n^{2}+\left(8\sqrt{5}-24\sqrt{2}\right)n+O(1),$$

and

$$\overline{SO}_{\text{red}}\left(CL_{n}\right)=4\sqrt{2}\,n^{2}-8\sqrt{2}\,n.$$

For the metric side,

$$\Theta\left(L_{n}\right)=\frac{3}{2}n^{2}+O(n), \qquad \Theta\left(CL_{n}\right)=n^{2}+O(n),$$

while

$$W\left(L_{n}\right)=\frac{2}{3}n^{3}+O\left(n^{2}\right), \qquad W\left(CL_{n}\right)=\frac{1}{2}n^{3}+O\left(n^{2}\right).$$

And this means closure will keep the linear growth class of edge-based indices but reduces the leading constants of the distance-based descriptors;

The energy asymptotes come from Theorem 5 and the Riemannian sum interpretation of the cosine sums:

$$\lim_{n\to\infty}\frac{E_\pi\left(L_n\right)}{n}=\frac{8}{\pi}\int_0^{\pi/3}\cos\theta\,d\theta+\frac{2}{3}=\frac{4\sqrt{3}}{\pi}+\frac{2}{3}.$$

The same limit holds for CL_n because its sampled angles become uniformly distributed on the circle and the same threshold decomposition applies:

$$\lim_{n\to\infty}\frac{E_\pi\left(CL_n\right)}{n}=\frac{1}{2\pi}\int_0^{2\pi}\left(\,|2\cos\theta+1|+|2\cos\theta-1|\,\right)d\theta=\frac{4\sqrt{3}}{\pi}+\frac{2}{3}.$$

For this reason, the finite-size value of graph-energy density differs between them while both have the same asymptotic graph-energy density. The leading term is equal since the edge modification only impacts a constant number of local degrees while the bulk spectrum sampling contains O(n) modes. The boundary effects thus come in as lower order, oscillatory corrections and disappear after rescaling by n.

From the standpoint of exact graph descriptors, the two families therefore provide a useful benchmark pair. They have the same order $2n$, almost the same size, and very similar visual structure. The only change is the closure of the rails. Yet this single change leaves a constant trace in the ordinary Sombor index, a linear trace in the reduced Sombor coindex, a quadratic trace in total eccentricity, a cubic trace in the Wiener index, and only an oscillatory $O(1)$ trace in the energy. Few graph pairs illustrate so clearly that different descriptor families measure genuinely different structural phenomena.

6. Conclusion

An exact descriptor analysis of the open and cylindrical ladder graphs is present in this paper. Using edge and nonedge partitions, parity-sensitive distance counting, and Cartesian-product spectra, closed-formulas are generated for Sombor-type indices and coincides; standard degree-based indices; eccentricity measures; the Wiener index; and adjacency graph energy.

Cyclic closure eliminates the 4 lower-degree boundary vertices, regularizes the structure of its complement and collapses long paths. Hence, the edge-based descriptors grow by controlled amounts, as reflected from the decrease of reduced coincides more severely and that the total eccentricity and Wiener index show reducing trends. This shows that the limits of graph-energy density for the two families differ only by a lower-order oscillatory term, because the adjacency graph energy changes in an equivalent way. For the associated identical-mass, identical-spring model, exact natural-frequency branches and a discrete dispersion relation are obtained via Laplacian spectra, while damping and loading data are required to produce the frequency-response matrix. That is, the graph–energy invariant does not encode physical vibrational energy.

Author contributions: Conceptualization, SIM and YN; methodology, YN and AV; software, PW and JL; validation, AV, TMK and MFAH; formal analysis, YN;

investigation, SIM and YN; resources, AV and MFAH; data curation, PW and JL; writing—original draft preparation, SIM and YN; writing—review and editing, YN, AV, PW, JL, TMK and MFAH; visualization, YN, PW and TMK; supervision, AV; project administration, YN and SIM. All authors have read and agreed to the published version of the manuscript.

Funding: No external funding was received for this study.

Institutional review board statement: Not applicable. This study did not involve humans or animals.

Informed consent statement: Not applicable.

Data availability statement: No external dataset was used. All numerical values and figures were generated directly from the closed formulas established in the paper.

Conflict of interest: The authors declare no conflict of interest.

AI use statement: For the writing of this paper, AI-based language tool for language improvement was only used by the authors. The mathematical results have not been analysed, interpreted or generated with the assistance of any AI tool. The authors independently reviewed and edited all outputs, and are fully responsible for the integrity of the work.

References

1. Gutman I, Furtula B, Öz MS. Geometric approach to vertex-degree-based topological indices: elliptic Sombor index, theory and application. International Journal of Quantum Chemistry. 2024; 124(2): e27346. doi: 10.1002/qua.27346
2. Das KC, Çevik AS, Cangul IN, et al. On Sombor index. Symmetry. 2021; 13(1): 140. doi: 10.3390/sym13010140
3. Cruz R, Gutman I, Rada J. Sombor index of chemical graphs. Applied Mathematics and Computation. 2021; 399: 126018. doi: 10.1016/j.amc.2021.126018
4. Liu H, Gutman I, You L, et al. Sombor index: Review of extremal results and bounds. Journal of Mathematical Chemistry. 2022; 60: 771–798. doi: 10.1007/s10910-022-01333-y
5. Liu H, Chen H, Xiao Q, et al. More on Sombor indices of chemical graphs and their applications to the boiling point of benzenoid hydrocarbons. International Journal of Quantum Chemistry. 2021; 121: e26689. doi: 10.1002/qua.26689
6. Rada J, Rodríguez JM, Sigarreta JM. General properties on Sombor indices. Discrete Applied Mathematics. 2021; 299: 87–97. doi: 10.1016/j.dam.2021.04.014
7. Ning W, Song Y, Wang K. More on Sombor index of graphs. Mathematics. 2022; 10(3): 301. doi: 10.3390/math10030301
8. Deng H, Tang Z, Wu R. Molecular trees with extremal values of Sombor indices. International Journal of Quantum Chemistry. 2021; 121(11): e26622. doi: 10.1002/qua.26622
9. Dorjsembe S, Horoldagva B. Reduced Sombor index of bicyclic graphs. Asian-European Journal of Mathematics. 2022; 15(7): 2250128. doi: 10.1142/S1793557122501285
10. Wang F, Wu B. The reduced Sombor index and the exponential reduced Sombor index of a molecular tree. Journal of Mathematical Analysis and Applications. 2022; 515: 126442. doi: 10.1016/j.jmaa.2022.126442
11. Phanjoubam C, Mawiong SM, Buhphang AM. On Sombor coindex of graphs. Communications in Combinatorics and Optimization. 2023; 8(3): 513–529. doi: 10.22049/CCO.2022.27751.1343
12. Du Z, You L, Liu H, et al. The Sombor index and coindex of chemical graphs. Polycyclic Aromatic Compounds. 2024; 44(5): 2942–2965. doi: 10.1080/10406638.2023.2225683
13. Rada J, Rodríguez JM, Sigarreta JM. Sombor index and elliptic Sombor index of benzenoid systems. Applied Mathematics and Computation. 2024; 475: 128756. doi: 10.1016/j.amc.2024.128756
14. Gutman I, Trinajstić N. Graph theory and molecular orbitals: Total π-electron energy of alternant hydrocarbons.

Chemical Physics Letters. 1972; 17(4): 535–538. doi: 10.1016/0009-2614(72)85099-1
15. McClelland BJ. Properties of the latent roots of a matrix: The estimation of π-electron energies. Journal of Chemical Physics. 1971; 54(2): 640–643. doi: 10.1063/1.1674889
16. Gutman I, Polansky OE. Mathematical Concepts in Organic Chemistry. Springer; 1986. doi: 10.1007/978-3-642-70982-1
17. Gutman I, Das KC. Estimating the total π-electron energy. Journal of the Serbian Chemical Society. 2013; 78(12): 1925–1933. doi: 10.2298/JSC130905092G
18. Jahanbani A, Sheikholeslami SM, Khoeilar R. On the energy of benzenoid hydrocarbons. Polycyclic Aromatic Compounds. 2022; 42(8): 5204–5216. doi: 10.1080/10406638.2021.1933103
19. Li X, Shi Y, Gutman I. Graph Energy. Springer; 2012. doi: 10.1007/978-1-4614-4220-2
20. Brouwer AE, Haemers WH. Spectra of Graphs. Springer; 2012. doi: 10.1007/978-1-4614-1939-6
21. Diestel R. Graph Theory, 5th ed. Springer; 2017. doi: 10.1007/978-3-662-53622-3
22. Godsil C, Royle G. Algebraic Graph Theory. Springer; 2001. doi: 10.1007/978-1-4613-0163-9
23. Mead DJ. A general theory of harmonic wave propagation in linear periodic systems with multiple coupling. Journal of Sound and Vibration. 1973; 27(2): 235–260. doi: 10.1016/0022-460X(73)90064-3
24. Hussein MI, Leamy MJ, Ruzzene M. Dynamics of phononic materials and structures: historical origins, recent progress, and future outlook. Applied Mechanics Reviews. 2014; 66(4): 040802. doi: 10.1115/1.4026911
25. Doyle JF. Wave Propagation in Structures: Spectral Analysis Using Fast Discrete Fourier Transforms, 2nd ed. Springer; 1997. doi: 10.1007/978-1-4612-1832-6
26. Movahedi F. Results on the elliptic Sombor index. RAIRO – Operations Research. 2025; 59(4): 2201–2212. doi: 10.1051/ro/2025086
27. Ahmad S, Das KC, Farooq R. On elliptic Sombor index with applications. Bulletin of the Malaysian Mathematical Sciences Society. 2025; 48: 108. doi: 10.1007/s40840-025-01894-6
28. Lin Z, Wang J, Wang Y. Geometric approach to degree-based topological index. International Journal of Mathematics. 2026; 37: 2650024. doi: 10.1142/S1793830926500242
29. Zhang W, Meng J, Wu N. Extremal graphs for Sombor index with given parameters. Axioms. 2023; 12(2): 203. doi: 10.3390/axioms12020203
30. Du Z, You L, Liu H, et al. The Sombor index and coindex of two-trees. AIMS Mathematics. 2023; 8(8): 18982–18994. doi: 10.3934/math.2023967
31. Aguilar-Sánchez R, Méndez-Bermúdez JA, Rodríguez JM, et al. Normalized Sombor indices as complexity measures of random networks. Entropy. 2021; 23(8): 976. doi: 10.3390/e23080976
32. Barman J, Das S. Geometric approach to degree-based topological index: hyperbolic Sombor index. MATCH Communications in Mathematical and in Computer Chemistry. 2026; 95: 63–94.